The Journal of Chemical Physics

RESEARCH ARTICLE | FEBRUARY 04 2015

Optically probing Al—O and O—H vibrations to characterize water adsorption and surface reconstruction on *α*-alumina: An experimental and theoretical study

Yujin Tong; Jonas Wirth; Harald Kirsch; Martin Wolf; Peter Saalfrank; R. Kramer Campen

J. Chem. Phys. 142, 054704 (2015)
https://doi.org/10.1063/1.4906346

Optically probing Al—O and O—H vibrations to characterize water adsorption and surface reconstruction on α-alumina: An experimental and theoretical study

Yujin Tong,[1,a)] Jonas Wirth,[2] Harald Kirsch,[1] Martin Wolf,[1] Peter Saalfrank,[2] and R. Kramer Campen[1,b)]
[1]*Fritz Haber Institute of the Max Planck Society, 14195 Berlin, Germany*
[2]*Institute of Chemistry, University of Potsdam, 14476 Potsdam OT Golm, Germany*

(Received 30 September 2014; accepted 7 January 2015; published online 4 February 2015)

Oxide/water interfaces are ubiquitous in a wide variety of applications and the environment. Despite this ubiquity, and attendant decades of study, gaining molecular level insight into water/oxide interaction has proven challenging. In part, this challenge springs from a lack of tools to concurrently characterize changes in surface structure (i.e., water/oxide interaction from the perspective of the solid) and O—H population and local environment (i.e., water/oxide interaction from the water perspective). Here, we demonstrate the application of surface specific vibrational spectroscopy to the characterization of the interaction of the paradigmatic α-Al_2O_3(0001) surface and water. By probing both the interfacial Al—O (surface phonon) and O—H spectral response, we characterize this interaction from both perspectives. Through electronic structure calculation, we assign the interfacial Al—O response and rationalize its changes on surface dehydroxylation and reconstruction. Because our technique is all-optical and interface specific, it is equally applicable to oxide surfaces in vacuum, ambient atmospheres and at the solid/liquid interface. Application of this approach to additional alumina surfaces and other oxides thus seems likely to significantly expand our understanding of how water meets oxide surfaces and thus the wide variety of phenomena this interaction controls. © *2015 AIP Publishing LLC.* [http://dx.doi.org/10.1063/1.4906346]

I. INTRODUCTION

Oxide surfaces are ubiquitous in the environment and in applications ranging from ceramics to electronics to catalysis.[1–4] Much previous work has shown that their properties (e.g., structure, surface speciation, and charge) change dramatically on interaction with water. Gaining molecular level insight into the relationship between interfacial water and oxide surface properties is challenging, in part, because the dissociative adsorption of water is thermodynamically favorable on many simple oxide surfaces. This dissociative adsorption leads to coupled changes in interfacial chemistry, as one O—H bond of (a fraction of) interfacial water molecules is broken, and in structure, as in response to surface hydroxylation, the relative positions of oxide surface metal and oxygen atoms often change dramatically. The reconstructed surface typically exposes hydroxyls whose acidity is a function of oxygen coordination to the underlying lattice.[5–7] Thus, at the oxide/liquid water interface, protons are accepted from or donated to the bulk liquid as a function of pH. This surface (de)protonation leads to macroscopic interfacial charge development and substantially increases the challenge in understanding the relationship between surface reactivity and structure.

To experimentally probe this structure/reactivity relationship, we would, ideally, like a tool that allows us to characterize *both* dissociated water *and* interfacial structure at oxide surfaces ranging from the ultra high vacuum (in the presence of just a few water molecules) to the oxide/liquid water interface as a function of pH. In principle, the study of well defined single crystal surfaces in the presence of low numbers of water molecules in vacuum allows the application of electron-in/electron-out techniques (e.g., low energy electron diffraction (LEED), electron energy loss spectroscopy (EELS), and Auger Electron Spectroscopy) to this problem. However, these methods are not generally applicable in the presence of moderate to high water pressures or at the solid/liquid interface and have been demonstrated in some systems, e.g., LEED at an α-alumina surface, to lead to surface dehydroxylation.[8]

In contrast to electron based spectroscopies, characterization of oxide surfaces in UHV, at high water pressures and in the presence of liquid water, can, in principle, be performed using scanning probe microscopies (SPM)[4] or x-ray scattering or diffraction based approaches.[9,10] However, while SPM techniques provide useful information about the local structure of surface atoms, they cannot generally be used to probe surface hydrogens, they do not directly probe the presence/absence of chemical bonds, and their application to oxide surfaces with atomic resolution, in the presence of liquid water, is challenging.[11,12] X-ray scattering or diffraction based techniques can offer precise information about surface relaxation and reconstruction but typically require spatial averaging in the plane of the surface (thus obscuring heterogeneity) and, as for SPM approaches, are insensitive to hydrogen. To summarize, most of the experimental approaches applied to understand oxide/water interaction are limited: they are insensitive

a)Electronic mail: tong@fhi-berlin.mpg.de
b)Electronic mail: campen@fhi-berlin.mpg.de

to hydrogen (or oxygen hydrogen covalent bonds) and are not applicable in ambient atmospheres or at the solid/liquid interface or spatially average.

In principle, vibrational spectroscopy can overcome these hurdles: performing spectroscopy at O—H stretch frequencies can elucidate the fate of water at the surface while probing interfacial metal-oxygen modes (i.e., surface phonons) can provide insight into the manner in which surface structure evolves after interaction with water. Further, if these modes are probed in a photon-in/photon-out manner, as in infrared absorption or spontaneous Raman spectroscopies, they are in principle equally accessible in UHV and in the presence of liquid water. Unfortunately, applying infrared absorption or spontaneous Raman at either O—H or metal-oxygen frequencies is challenging because of their lack of interfacial specificity and the relatively low reflectivity of oxide surfaces in the infrared.[13,14] The former problem is particularly acute: the optical activity of the bulk lattice will always overwhelm that of interfacial metal-oxygen modes and, at the oxide/liquid water interface, similar difficulties apply in distinguishing the interfacial O—H stretch response from that of water molecules in bulk. Vibrational Sum Frequency (VSF) spectroscopy is a laser-based nonlinear optical technique that is prohibited, within the dipole approximation, in media with inversion symmetry. Because inversion symmetry must be broken at interfaces, in two phase systems in which both bulk phases are inversion symmetric, VSF spectroscopy furnishes the vibrational spectra of just the 1-2 layers of molecules near an interface.[15] This requirement for inversion symmetry breaking also applies on the microscopic level: for an individual mode to be VSF active, it must be *both* infrared (IR) *and* Raman active (see below for further discussion).

Inspired by its attractive selection rules, VSF spectroscopy has been employed by a number of investigators to characterize a wide variety of interfaces.[16–28] Of most direct relevance to this work, using VSF spectroscopy, several groups have probed the O—H stretch spectral range at both the oxide/ambient air and oxide/liquid water interfaces as a function of pH.[29–36] While useful, this interfacial O—H stretch spectral response alone can be challenging to interpret—it is often difficult to distinguish the spectral response of OH groups covalently bound to the surface that donate a hydrogen bond (to another surface oxygen or an interfacial water) from that of an OH on an intact interfacial molecular water that also does—and provides no direct insight into surface structure. In principle, probing interfacial metal-oxygen modes, i.e., surface phonons, can provide such surface structural insight.

Recently, Shen and coworkers have demonstrated the application of VSF spectroscopy to probing interfacial Si—O modes at the air/α-SiO_2(0001) and air/fused silica interfaces.[37] While they observed clear VSF spectral features in a frequency range in which Si—O modes are known to absorb, i.e., 800–1150 cm^{-1} and saw this spectral response change under moderate heating, assigning these spectral changes to specific changes in surface structure proved challenging. This challenge was, in part, due to the samples chosen to study: α-quartz and fused silica. The former is not inversion symmetric and is thus bulk VSF active, and both interfaces show substantial heterogeneity in surface oxygen types (with respect to coordination to the underlying lattice) and thus possible differences in Si—O spectral response. Such heterogeneity makes assignment of the microscopic origin of each resonance through comparison to calculation difficult. Finally, because the O—H spectral response was not monitored in these experiments, understanding how changes in interfacial Si—O spectral response correlate with water dissociative adsorption was not possible.

In this study, we connect the interfacial metal-oxygen spectral response to water dissociative adsorption and provide an atomically resolved view of how these modes relate to surface atom displacements. We focus on the interaction of the α-Al_2O_3(0001) surface with water in ambient air. α-Al_2O_3 is ubiquitous in a wide variety of applications and is a useful model for more complicated environmentally abundant alumino-silicate phases.[38,39] In addition, this surface has two significant practical advantages: (1) because bulk α-Al_2O_3 *is* inversion symmetric, there is no VSF response from the bulk crystal. This makes evaluation of the symmetry of the Al—O surface response straightforward and (2) as has been previously demonstrated, the hydrated α-Al_2O_3(0001) surface in air shows a clear non-hydrogen bonded OH resonance that originates from the OH stretch vibration of surface aluminols: a clear spectroscopic marker of water dissociative adsorption. To characterize how hydroxylation happens on this surface in ambient air, we probe the interfacial Al—O and O—H spectral responses of two well-defined surface structures—the Al-terminated, fully dehydroxylated surface and the fully hydroxylated surface—and probe how moderate heating explores structures intermediate between these end members. As we will show in detail, probing well defined structural end members enables straightforward comparison to calculated normal modes characteristic of each surface termination and, thus, assignment of all observed resonances by comparison with calculation.

By probing these two frequency regimes, we extract a complementary picture of the effect of water dissociative adsorption on the α-Al_2O_3(0001) surface. Both as seen from the perspective of the adsorbing water molecule, in the OH stretch spectral response, and from the evolving surface structure, in the Al—O response, water dissociative adsorption and concurrent surface reconstruction are thermodynamically favorable outside of UHV but slow (i.e., weeks). The approach we demonstrate here is fully general both with respect to oxide composition and polymorph, e.g., other Al_2O_3 , Fe_2O_3, or TiO_2 surfaces might be probed equally easily, and local density (or chemical potential) of water, i.e., it can be straightforwardly applied to oxide surfaces in UHV and those in contact with liquid water. As a result of this generality, and because this combination of concurrent insight into water structure and reactivity and oxide surface structure is unavailable by other means, we expect the combined experimental/computational approach we describe should be of wide interest to those interested in oxide/water interaction or the processes such interactions control.

II. METHODS

A. VSF measurement

To perform a VSF measurement, we temporally and spatially overlap a spectrally broad infrared pulsed laser with a

spectrally narrow pulsed visible laser and monitor the emission at the sum of the frequencies of the two incident fields. To create the two incident fields, we employ a laser system composed of a Ti:Sapphire oscillator (Venteon, Femtosecond Laser Technologies) and regenerative amplifier (Legend Elite Due HE+ Cryo PA, Coherent). One half of the regenerative amplifier output (7.5 mJ/pulse, 45 fs pulses, 1 kHz, centered at 800 nm) is used to pump a commercial optical parametric amplifier (HE-TOPAS, Light Conversion) the signal and idler output of which are mixed, in a non-collinear DFG scheme, to produce the IR. The center frequency of the IR beam was tuned to 3636 cm^{-1} for probing the interfacial O—H stretch and 800 cm^{-1} for probing of interfacial Al—O. To generate the narrowband visible (VIS) pulse, we used the residual 800 nm light from the OPA and a home-made pulse shaper. The resulting beam was, for the Al—O measurements, centered at 767 nm with a bandwidth of 32 cm^{-1} and, for the O—H, at 800 nm with a bandwidth of 22 cm^{-1}. The energy per pulse of the IR and VIS at the sample surface was 5.8 and 25.4 μJ for the Al—O stretch frequency region and 14 and 27 μJ for O—H stretch region, respectively. Polarizations and energies of the incident fields at the interface were controlled using $\lambda/2$ plate, polarizer, $\lambda/2$ plate combinations. The two beams were directed so as to propagate in the x-z plane (see Figure 1 for coordinate system) and focused on the samples using lenses with focal lengths of 10 and 45 cm and incident angles of $40.4° \pm 0.5°$ and $65° \pm 0.5°$ for the IR and VIS in the low frequency measurements and $59° \pm 0.5°$ and $39° \pm 0.5°$ for the IR and VIS in the high. After collimation, the VSF signal was dispersed in a spectrograph (SR303i, Andor Technology) and imaged on an electron multiplying charge coupled device (EMCCD) camera (Newton, Andor Technology). All measurements were conducted in ambient conditions at room temperature and under the *ssp* polarization condition (*s*-polarized SF, *s*-polarized visible, and *p*-polarized IR where *p* indicates polarization in the x-z plane and *s* polarization orthogonal). The acquisition time for spectra of a gold thin film reference, z-cut quartz reference, and α-Al_2O_3 were 30, 30, and 300 s, respectively. Non-resonant signals from the gold and z-cut quartz references were used to correct for the frequency dependent IR intensity for Al—O stretching and O—H stretching frequency regions, respectively. The gold film was employed as the low frequency IR energy reference because bulk z-cut quartz contains VSF active Si—O modes in this spectral window.[37,40]

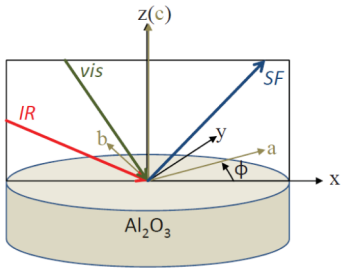

FIG. 1. Experimental geometry. All beams are in the x-z plane. VSF spectra were collected at different angles between the x-z plane and a-c plane of the α-alumina sample. This angle is defined as the azimuthal angle (ϕ). See text for further discussion.

B. Sample preparation

To prepare the Al-terminated, dehydroxylated sample, we modified previously published recipes.[8] In brief, we took a single crystal of α-Al_2O_3(0001) purchased from either UAB Altechna or Princeton Scientific (all results were verified independent of vendor), sonicated it in methanol for 15 min, dried it with N_2, and then washed it with milli-Q H_2O (18.3 MΩ cm). After washing, the crystal was mounted in a UHV chamber where it was Ar ion sputtered with 1.5 kV and annealed in O_2 at 1040 K. LEED and Auger Electron spectroscopy verified that, after this treatment, this surface had the characteristic (1×1) pattern of the 1-Al terminated α-Al_2O_3(0001) surface (see further discussion of this point below) and no discernible (within the sensitivity of our Auger spectrometer, <1% of a monolayer) carbon contamination. After preparation, this crystal *was removed* from the UHV chamber for VSF characterization in air. Both surface contamination by adventitious carbon and reaction with water vapor in the lab air are thus possible before analysis. We addressed the first possible problem by collecting VSF spectra of the C—H, C═O, and C═C spectral regions. These results suggest no significant carbon adsorption in the first 24 h. After this period, an interfacial C—H spectral response was visible. However, heating the sample to 350°C in air for 30 min removed this peak with no observable effect on either the Al—O or O—H interfacial spectral response. As is discussed in detail below, we constrained the second possible problem by collecting VSF spectra in the Al—O and O—H frequency regimes as a function of time after removal from vacuum. These time series suggest that our UHV prepared surface is sufficiently stable that more than one month of reacting with lab air would be required before the spectral response in either range significantly changed.

To prepare the fully hydroxylated surface, we took the as received sample, cleaned it in a sonication bath with acetone for 15 min, ethanol for 15 min, and Milli-Q water (18.3 MΩ cm) for 45 min. The sample was then mildly acid etched using a 15 mM solution of HNO_3 under sonication for 30 min and, after thoroughly rinsing with Milli-Q water, dried by blowing with nitrogen gas. No C—H or C═O stretch peaks were observed in the VSF response of the cleaned surface.

C. Spectral modeling

To quantify the observed VSF spectral response, a line shape model is required that relates the experimentally controllable parameters to the frequency dependent macroscopic material response (i.e., the second order nonlinear susceptibility).[40–42] Much prior work has shown that this relationship is a function of the macroscopic symmetry of the interface. As will become clear below, the interfacial O—H stretch response has $C_{\infty v}$ symmetry (no dependence on aziumthal angle, see Figure 1) while some of the spectral features apparent in the Al—O response have C_{3v} (three fold symmetry with respect to azimuthal angle). The appropriate expression for the C_{3v} surface interrogated under the *ssp* polarization condition is[40]

$$I^{ssp}_{VSF}(\tilde{\nu}_{SF}) \propto |L_{yy}(\tilde{\nu}_{SF})L_{yy}(\tilde{\nu}_{VIS})[L_{xx}(\tilde{\nu}_{IR}) \cos\theta_{IR}\chi^{(2)}_{yyx} + L_{zz}(\tilde{\nu}_{IR}) \sin\theta_{IR}\chi^{(2)}_{yyz}]|^2$$

$$\propto |L_{yy}(\tilde{\nu}_{SF})L_{yy}(\tilde{\nu}_{VIS}) \times [-L_{xx}(\tilde{\nu}_{IR})\cos\theta_{IR}\chi^{(2)}_{aaa}\cos 3\phi + L_{zz}(\tilde{\nu}_{IR})\sin\theta_{IR}\chi^{(2)}_{aac}]|^2, \quad (1)$$

and for a surface of $C_{\infty v}$ symmetry is[42]

$$I^{ssp}_{VSF}(\tilde{\nu}_{SF}) \propto \left|L_{yy}(\tilde{\nu}_{SF})L_{yy}(\tilde{\nu}_{VIS})L_{zz}(\tilde{\nu}_{IR})\sin\theta_{IR}\chi^{(2)}_{yyz}\right|^2 \propto \left|L_{yy}(\tilde{\nu}_{SF})L_{yy}(\tilde{\nu}_{VIS})L_{zz}(\tilde{\nu}_{IR})\sin\theta_{IR}\chi^{(2)}_{aac}\right|^2, \quad (2)$$

where $I^{ssp}_{SF}(\tilde{\nu}_{SF})$ is the normalized VSF intensity measured under the *ssp* polarization condition, $L_{ii}(\tilde{\nu}_{\alpha})$ the local Fresnel factor for beam $\alpha(\alpha = \text{SF, IR, or VIS})$, which is a function of the experimental geometry and the refractive index of the mediums (the appropriate expressions have appeared in a variety of prior studies, e.g., the review of Wang and coworkers[21]), θ_{α} is the incident angle for beam α, and $\chi^{(2)}_{ijk}$ is the ijkth element of the second order susceptibility tensor, which depends on the molecular hyperpolarizability and orientation. For our C_{3v} surface, the material centered macroscopic coordinate system is not equivalent to the laboratory reference frame. In Eq. (1), the indices xyz indicate a quantity in the lab frame, abc a quantity in the material centered frame, and ϕ the azimuthal angle of the sample with respect to the beams' incident plane (see Figure 1) that defines their relationship. The zero of ϕ is determined by rotating the crystal such that the (0001) and (1120) axes are in the plane of the incident beams. This orientation is verified via external markings indicated by the vendor and minima/maxima in the observed I_{VSF}. As indicated in Eq. (2), for an interface of $C_{\infty v}$ symmetry, the two coordinate systems are coincident. Equations (1) and (2) assume, as has been demonstrated to be generally true for dielectrics,[43] that the so-called quadrupole contribution to the observed I_{VSF} is minimal. The appropriate expressions for spectra resulting from samples interrogated under other polarization conditions are reproduced in the supplementary material.[89]

Following prior workers, we describe $\chi^{(2)}_{ijk}$ as a coherent superposition of a nonresonant background and Lorentzian resonance(s),[44]

$$\chi^{(2)}_{ijk} = \chi^{(2)}_{nr} + \chi^{(2)}_{r} = |\chi_{nr}|e^{i\epsilon} + \sum_n \frac{\chi_{n,ijk}}{\tilde{\nu}_{IR} - \tilde{\nu}_n + i\Gamma_n}, \quad (3)$$

where $\tilde{\nu}_{IR}$ is the frequency of the incident infrared; $|\chi_{nr}|$ and ϵ are the nonresonant amplitude and phase; and $\chi_{n,ijk}$, $\tilde{\nu}_n$, and Γ_n are the complex amplitude, center frequency, and line width of the n^{th} resonance (see supplementary material justification of this choice of line shape model[89]). To actually analyze the data, we substitute Eq. (3) into either Eq. (2) or (1) and fit the measured VSF spectrum using the Levenberg-Marquardt algorithm as implemented in the commercial visualization and analysis program Igor Pro (Wavemetrics) (further discussion of data analysis is in the supplementary material[89]). Because all parameters in Eq. (3) are independent of azimuthal angle, when analyzing the Al—O response, we conducted a global fit of a series of spectra as a function of ϕ. It is also worth noting that for VSF measurement of the Al—O response correction for the Fresnel factors at IR frequencies (i.e., $L_{ii}(\omega_{ir})$) is critical. As is clear from the literature tabulations,[45–47] in this frequency range, the linear dielectric constants of α-Al_2O_3 change by several orders of magnitude. This leads, as shown in the supplementary material,[89] to a several order of magnitude change in L_{ii} in our frequency region of interest.

D. First-principles calculations

Periodic first-principles total energy calculations were performed within the framework of Kohn-Sham density functional theory (DFT)[48] applying the projector augmented wave (PAW) method[49,50] as implemented in the Vienna *ab initio* simulation package (VASP).[51–53] Electron exchange and correlation were treated according to the generalized gradient approximation (GGA) using the PBE functional.[54,55] Total energies were corrected for dispersion interaction using Grimme's semiempirical D2 scheme.[56] Total energies and vibrational frequencies were evaluated using a plane-wave basis set truncated at a kinetic energy cutoff of 400 eV and a Γ-point centered (5×5×1) Monkhorst-Pack grid[57] (resulting in a set of 13 irreducible k-points) for sampling the Brillouin zone of the hexagonal unit cell. Self-consistent field convergence was considered to have occurred for a total energy difference of less than 10^{-4} eV between iterations; ionic relaxation was stopped when the forces acting on ions dropped below 0.01 eV/Å.

Bulk α-alumina has a hexagonal unit cell with alternating layers of aluminum and oxygen atoms stacked along the [0001] direction, as shown in Figure 2(a). After geometry optimization, we found bulk lattice constants of $a = b = 4.83$ Å and $c = 13.09$ Å. These values exceed those found in experiment[58] by a GGA-typical amount of approximately 1%.

Both the Al-terminated and the fully hydroxylated (0001) surface were modeled using exceptionally thick slabs based on two α-alumina unit cells along the (0001) direction, resulting in 36 atomic layers (counting the displaced hydrogen atoms as one layer) and identical surfaces on both sides of the slabs (see Figures 2(b)–2(d)). While the structure of the Al-terminated surface is uniquely defined, in the hydroxyl-

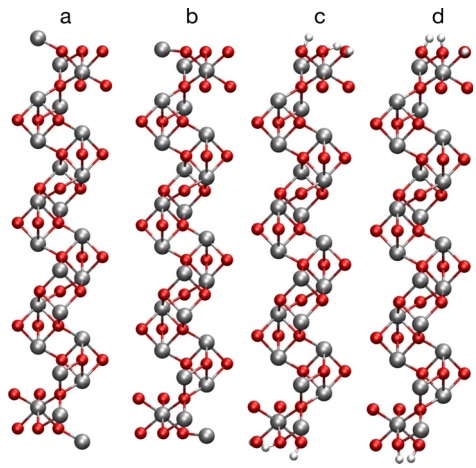

FIG. 2. (a) Model used to calculate bulk α-Al_2O_3 properties. (b) Slab used to calculate Al-terminated, UHV-prepared, α-Al_2O_3(0001) surface properties. ((c) and (d)) Slabs used to calculate hydroxylated α-Al_2O_3(0001) surface properties; (c) contains two intra-aluminol hydrogen bonds (config. 2), and (d) contains only one (config. 1).

ated case, different configurations of surface OH groups are possible; thermal fluctuations between distinct configurations have been shown to occur at room temperature.[59] In most previous studies, a (1×1) structure with respect to the surface unit cell, featuring one hydrogen bond between surface aluminols (config. 1, see Figure 2(d)), was used as a model of the ideal termination.[59–61] Here, we also consider a second configuration with two hydrogen bonds between aluminols (config. 2, see Figure 2(c)) that is isoenergetic. Note, however, that these models can only serve as examples of more complex (possibly non-periodic) patterns ranging over multiple surface unit cells.

The large slab thickness we employ facilitates the distinction between bulk and surface phonons. Fortuitously, the inversion symmetry of α-alumina generates a vanishing dipole moment of the cell, avoiding dipolar interactions between neighboring slabs. A vacuum gap of approximately 26 Å was found to ensure convergence of total energies within a few meV; pairwise dispersion interactions were limited to distances smaller than 20 Å to avoid interference between adjacent slabs. Molecular vibrations were calculated by normal mode analysis, i.e., by diagonalization of the dynamical (Hessian) matrix. Energy derivatives with respect to the nuclear coordinates were evaluated numerically using centered finite differences; all nuclear degrees of freedom were included. Normal mode analysis yields 180 and 192 vibrations for the Al-terminated and both fully hydroxylated (0001) surface models, respectively. Since there is no unique way to select predominantly surface related modes out of this pool, we introduce a phenomenological criterion: we consider a vibration to be a surface phonon if the corresponding normal mode exhibits an average ionic displacement vector $\langle \Delta q_{\text{surf}} \rangle$ for surface atoms that is longer by a factor F than the respective vector $\langle \Delta q_{\text{bulk}} \rangle$ for bulk atoms

$$\langle \Delta q_{\text{surf}} \rangle > F \langle \Delta q_{\text{bulk}} \rangle. \tag{4}$$

We systematically tested different values for F and different atomic layers as frontiers between *bulk* and *surface*, arriving at $F = 4$ and the definition of all but the uppermost four layers as bulk layers. This criterion (see supplementary material for more details[89]) gives sufficiently stable results with respect to variation of both parameters and a selection of modes that is consistent with the experimental observations.

III. RESULTS AND DISCUSSION

A. VSF Al—O response of the hydrated α-Al_2O_3(0001) surface

The VSF response for the hydrated α-Al_2O_3(0001) surface is shown in the upper panel of Figure 3 for $\phi = 20°$ and 80° (see Figure 1 for the definition of ϕ) between 700 and 1000 cm^{-1}. Two qualitative features of the data are immediately apparent: (i) two apparent peaks dominate the spectral response and (ii) the observed spectral features are clearly azimuthal angle dependent: at $\phi = 20°$, a broad peak is apparent at 875 cm^{-1} with a dip at 750 cm^{-1} while at $\phi = 80°$, the 875 cm^{-1} peak disappears and the 750 cm^{-1} dip becomes a peak. Similar measurements (spectra shown in the supplementary material[89]) with ϕ ranging from 0° to 360° show that this trend repeats with a periodicity of 120° and that the two peaks are out of phase by 180°. Both features of these data can be readily appreciated by extracting the integrated VSF intensities from 700 to 800 cm^{-1} and 800 to 920 cm^{-1} and plotting as a function of ϕ (see inset in Figure 3).

As tabulated in a variety of standard references, α-Al_2O_3 belongs to the D_{3d} point group.[62] Crystals from this group have inversion symmetry in bulk. As a result, there are no bulk optical modes that are both IR and Raman active.[45,47,63,64] As discussed above, in order for a mode to be VSF active, local inversion symmetry must be broken: it must be both IR and Raman active.[15] This strongly suggests that bulk α-Al_2O_3 does not contribute to our observed signal. Further, in analogy to previous studies of a D_3 point group crystal terminated along its (0001) plane,[37] the α-Al_2O_3(0001) surface should have symmetry C_{3v} or higher. For such a surface, four independent,

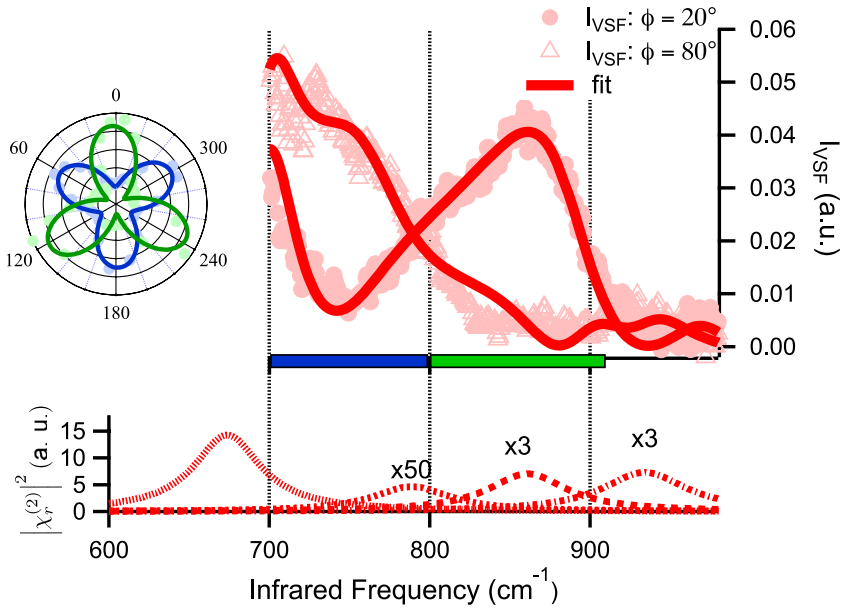

FIG. 3. Representative VSF spectra in Al—O stretch region of the hydrated α-Al_2O_3(0001) surface with azimuthal angle $\phi = 20°$ (filled circles) and $\phi = 80°$ (open triangles); red solid lines are the global fit spectra with the line shape model of Eqs. (1) and (3). Bottom panel: resonances extracted from the global fitting. While the lowest frequency resonance, centered at 674 cm^{-1}, is outside of the measured spectral window, its effect on the measured spectra is clear by interference with the other modes. Inset: Polar plot of integrated VSF intensities (open circles) for the indicated frequency regions (blue and green bars on the bottom axis in top figure). Solid blue and green lines are the result of fits to Eqs. (1) and (3).

non-zero $\chi^{(2)}$ components are possible of which three are isotropic (i.e., A modes) and one anisotropic (E modes) with apparent three fold symmetry.[37,65,66] Clearly, both the presence of an observable VSF response (requiring both Raman and IR activity) and the three-fold symmetry of the response strongly suggest a surface origin of the observed signal.

Given the signal's surface origin, the three fold symmetry of both apparent peaks with respect to azimuthal angle and their phase difference, we employed the line shape model in Eqs. (1) and (3) to quantify the spectral response (assuming rotating the sample changes only the azimuthal angle ϕ and not the resonant or nonresonant response; see supplementary material for detailed discussion of the fitting procedure[89]). This analysis results in four peaks, centered at 934 ± 8 cm^{-1},861 ± 2 cm^{-1}, 789 ± 2 cm^{-1}, and 674 ± 5 cm^{-1}. As reference to Eq. (1) shows, the measured I_{SF}^{ssp} is a function of both the *aac* and *aaa* elements of the macroscopic nonlinear susceptibility. As shown in the supplementary material in detail,[89] $\chi^{(2)}_{aac}$ is dominated by the two high frequency resonances while $\chi^{(2)}_{aaa}$ is dominated by the lowest frequency mode.

Several features of this analysis are worth noting in further detail. First, as described in detail in the supplementary material,[89] the resonance centered at 934 cm^{-1} also appears in spectra collected under *psp*, *pps*, and *spp* polarization conditions. Presumably, the absence of other modes under these polarizations is due either to local orientational effects[21] or the relatively low nonresonant response in these configurations that thus removes the self-heterodyning apparent under *ssp*.[37] Second, while the resonance at 674 cm^{-1} is outside of our measured spectral window, its presence is quite clear from the significant interference with the higher frequency peaks apparent in the spectra collected as a function of ϕ.

Based on the observed symmetries of the VSF response and the structural symmetry of the α-Al_2O_3 bulk, it seems clear that we have observed the surface Al—O modes of the hydroxylated α-Al_2O_3(0001) surface. To provide an additional demonstration of the interfacial specificity of our approach, and help in the assignment of the observed spectral features, we next characterized the 1-Al terminated, fully dehydroxylated, surface.

B. VSF response of the Al-terminated surface

From a crystallographic point of view, an α-Al_2O_3(0001) surface has three possible terminations: two distinct aluminum and one oxygen.[67] A variety of experimental and computational studies have found that, in the absence of water, one of the Al terminations, the so-called 1-Al, is the most stable.[9,67,68] Such an Al terminated surface would be expected to have both a dramatically different surface Al—O spectral response than the hydroxylated surface (surface structure has changed) and a decreased interfacial OH response (less dissociated water). Figure 4 shows representative VSF measurements for an α-Al_2O_3(0001) sample prepared under UHV and removed from the chamber for VSF analysis in both the Al—O (Figure 4(a)) and O—H spectral regions (Figure 4(b)). For comparison, VSF spectra for the fully hydroxylated samples are also shown. As expected, the spectral response of the UHV prepared α-Al_2O_3(0001) surface differs dramatically

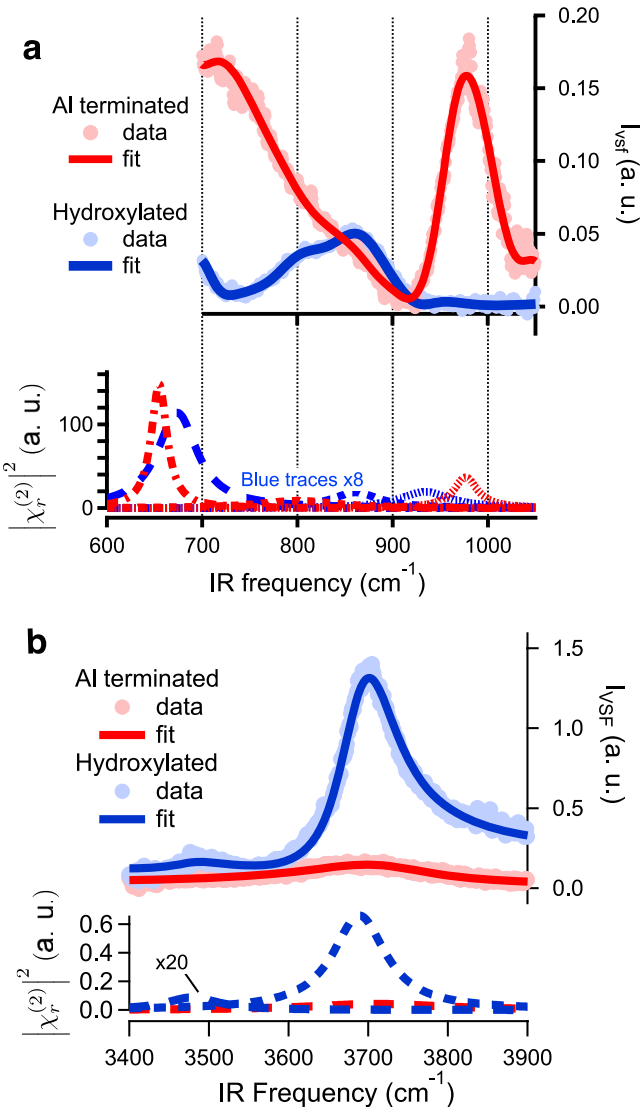

FIG. 4. (a) VSF spectra in low frequency region of UHV prepared α-Al_2O_3(0001) surface (red circles) and fully hydrated surface (blue circles) at $\phi = 0°$. Solid lines are the fits with the line shape model of Eqs. (1), (2), and (3). Reconstructed resonances from the fitted parameters are shown in the bottom panel. The resonances of the hydroxylated surface are as shown in Figure 3. All resonances extracted from the hydroxylated sample's spectral response, shown in dashed blue lines, are multiplied by 8× to allow plotting on the same scale as the Al-terminated. (b) VSF spectra in the O—H stretch region for the corresponding samples with extracted resonances shown in the lower panel. The lower frequency resonance of the hydroxylated samples is multiplied 20× to make it visible on the common scale.

from the hydroxylated in both frequency regions. In the low frequency region (Figure 4(a)), an intense peak is observed at 980 cm^{-1} with a broad intense feature increasing from 900 to 700 cm^{-1}. Neither of these two features are azimuthal dependent (data not shown). Quantifying the measured response with our line shape model (red solid line in Figure 4(a)) suggests that there are three resonances underlying the measured response centered at 655, 800, and 977 cm^{-1} (bottom panel of Figure 4(a)). Details of this fitting, uncertainty estimates, and demonstration that line shape models with fewer resonances systematically fail at describing the data are shown in the supplementary material.[89] In the OH stretch region (see Figure 4(b)) for the hydroxylated sample we clearly observe,

in quantitative agreement with a prior study by Shen and coworkers,[34] a single intense peak centered at 3700 cm^{-1} with a low intensity peak at lower frequencies. In contrast, the UHV prepared sample spectral response is dramatically weaker and broader. Quantifying this response results in a single, low amplitude mode centered at 3680 cm^{-1} with a full width half maximum of 150 cm^{-1} (bottom panel in Figure 4(b), see supplementary material for other fit parameters[89]). The low integrated intensity of this mode is clearly consistent with our expectations of low populations of dissociatively adsorbed water on this surface.

While the 1-Al terminated surface is thermodynamically stable in UHV, much prior work has shown that the dissociative adsorption of water, and subsequent surface reconstruction, is thermodynamically favorable under ambient conditions.[38,59] In light of this prior work, it is perhaps surprising that the spectral response of our α-Al_2O_3(0001) surface prepared in UHV but analyzed in ambient, and thus exposed to a partial H_2O pressure of ≈8.5 Torr in lab air, differs so dramatically from that of the fully hydrated sample. In fact, control experiments in the O—H stretch region suggest that more than 20 days of lab air exposure is necessary to see the O—H stretch spectral response of the UHV prepared sample increase significantly. Evidently, the kinetics of dissociative water adsorption and attendant surface reconstruction of α-Al_2O_3(0001) are slow.

Some prior workers have argued, based principally on TDS and XPS measurements, that water dissociatively adsorbs on the α-Al_2O_3(0001) surface after exposure to water partial pressures of ≈1 Torr for 20 min.[69–72] Clearly, our UHV prepared surface is dramatically less reactive. Three possible scenarios seem likely to explain the differences in reactivity concluded from that work and ours: adsorption of (e.g., hydrocarbon) contaminants on our samples dramatically slows water adsorption and reaction, a high concentration of defects on samples employed in previous work dramatically increased water reactivity, or the different preparation methods employed in each study of UHV prepared α-Al_2O_3(0001) have sampled different α-Al_2O_3(0001) terminations.

As discussed in Sec. II, we addressed the first scenario by performing control experiments in which we measured the VSF response of the UHV prepared sample in ambient in the C—H, C═O, and C═C stretch regions; no discernible spectral response was observed up to 24 h after sample creation. Consistent with carbon contamination not explaining this low reactivity, we have investigated similarly prepared α-Al_2O_3(0001) surfaces without removal from UHV (in the OD stretch frequency region) and found similarly low reactivity.[73]

While the fully hydroxylated *gibbsite-like* surface is not the most thermodynamically stable in UHV[67,74] transforming this surface, presumably containing adventitious carbon, to the pristine, thermodynamically stable 1-Al surface termination can be challenging as it requires removing surface carbon, dehydroxylating the surface and then removing one Al_2O_3 layer. Different authors have done this differently: Liu *et al.* simply heated the *as-purchased* α-Al_2O_3(0001) surface in UHV,[69] Kelber and coworkers both Ar^+ sputtered using various voltages and annealed the sample at high temperatures in O_2 to heal any sputtering induced oxygen vacancies,[70,71] and Fu *et al.* heated the sample in UHV, dosed water and then treated it with O_2 plasma to remove carbon. Our preparation procedure most closely resembles that of Kelber and coworkers but with longer sputtering times. Calculation clearly suggests that, for the three possible dehydroxylated surface terminations of α-Al_2O_3(0001), the 1-Al is, by far the most stable.[67] Thus, one possible explanation of the reduced reactivity that we observe is that our preparation methods produces this surface while others produce either other surface terminations, e.g., the oxygen terminated, or significant populations of reactive surface defects. Particularly in the case of those authors who prepare their sample by sputtering without subsequently annealing in O_2, the latter possibility seems likely. We are currently working to characterize surface terminations in UHV unambiguously by extending our surface phonon characterization over larger frequency ranges. For our purposes here, however, it is sufficient to note that the slow kinetics of surface transformation mean that removing our sample from the vacuum chamber has minimal influence on our spectral observables.

The Al terminated α-Al_2O_3(0001) surface has been previously studied in vacuum using LEED and high resolution electron energy loss spectroscopy (HREELS). Based on quantitative modeling of LEED data collected over 80-370 eV, Soares and coworkers concluded that, for this termination, surface aluminum atoms have anomalously large vibrational amplitudes at room temperature.[68] The relatively large VSF intensities of the Al—O modes on our UHV prepared α-Al_2O_3(0001) surface are consistent with their findings. In HREELS studies, a strong resonance has been observed between 800 and 880 cm^{-1} by several workers:[75] ≈80 cm^{-1} lower in energy than the mode apparent in the VSF data. Much prior work has shown that in polar semiconducting or insulating materials, the high frequency HREELS response is dominated by so-called Fuchs-Kliewer (FK) phonons whose frequencies are coincident with that at which the real part of the bulk dielectric function is −1 (i.e., $\mathrm{Re}(\epsilon_B) = -1$).[76,77] As discussed in more detail in the supplementary material, this clearly implies that for the Al terminated α-Al_2O_3(0001) the observed HREELS resonance results from the bulk α-Al_2O_3 crystal.[75,78,89] VSF is, as discussed in detail by Shen and coworkers in the context of the silica/air interface, insensitive to such FK phonons.[40]

C. Comparison of VSF response with calculated normal modes

We have thus far shown the result of probing interfacial Al—O modes at the α-Al_2O_3(0001) surface and that this surface phonon response changes dramatically after surface structure modification via dehydroxylation. Armed with this insight, we would next like to understand the microscopic changes in surface structure responsible for the changing Al—O spectral response. To do so, we took advantage of our well defined surface terminations, employed periodic DFT, and performed normal mode analyses for idealized models of both the 1-Al terminated (0001) surface—known to be thermodynamically most stable under UHV[67]—and the two fully hydroxylated *gibbsite-like* surfaces[61,79,80] (see Figure 2) that we found to be equivalently favorable. The results of these calculations are shown in Figure 5. While empirical scaling

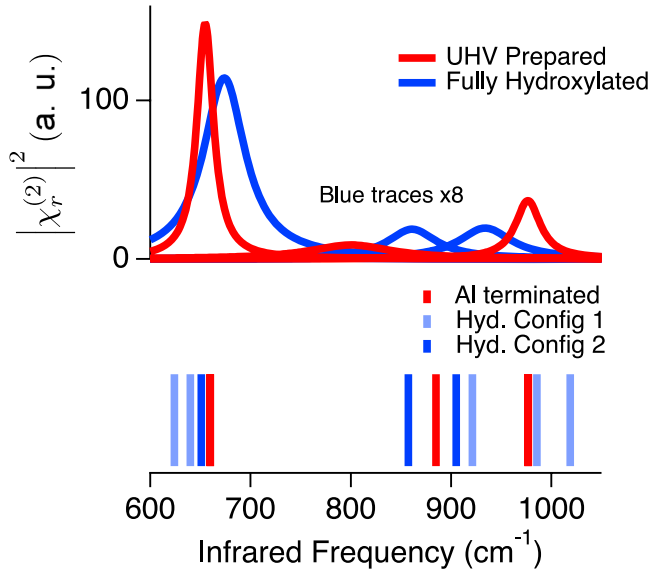

FIG. 5. (a) Top panel, extracted resonances, $|\chi_r^{(2)}|^2$ for the UHV prepared (red) and fully hydrated (blue) α-Al_2O_3(0001) surfaces (b). Simulated surface normal modes for Al-terminated (red stick) and O(H)-terminated α-Al_2O_3(0001) surfaces (see supplementary material for details regarding definition of surface normal modes[89]).

factors of harmonic frequencies, to account for model error and mode anharmonicity, are well documented in molecules, there has been much less work along these lines for modes on solid surfaces (for a detailed discussion of this point see supplementary material of our previous work[73]). Absent a well defined scaling factor for surface Al—O vibrations, we have assumed that the highest frequency calculated normal mode of the Al-terminated surface, i.e., 908/909 cm^{-1}, corresponds to the resonance observed in experiment at 977 cm^{-1} and that all calculated normal modes should be similarly scaled by a factor of 1.075 (*n.b.* the notation 908/909 should be taken to indicate that there are calculated normal modes whose frequencies differ by < 1 cm^{-1} and whose displacements are qualitatively identical). We opted to scale the data using this mode as a reference because it is separated by approximately 80 cm^{-1} from the next lower in frequency and is the most prominent mode that results from terminating the bulk. Lacking a similarly reliable assignment for the hydroxylated surface, we apply the same scaling factor in that case. In the following analysis, only scaled frequencies will be discussed.

As shown in Figure 5 in red, for the UHV prepared, Al-terminated α-Al_2O_3 (0001) surface normal modes are present at 659/660, 885, and 976/977 cm^{-1}. Given the equivalence at 977 cm^{-1}, calculated phonon frequencies at 659 and 660 cm^{-1} agree well with the experimental resonance at 655 cm^{-1} while the discrepancy between the frequency of the weak mode apparent in experiment at 800 cm^{-1} and the calculated normal mode at 885 cm^{-1} is larger. The displacement vectors for the 659, 885, and 976 cm^{-1} motions are shown in Figure 6 (displacements of the 660 and 977 cm^{-1} modes are shown in the supplementary material[89]). Clearly, the 976/977 modes are dominated by large amplitude motion of the surface Al atoms, the 885 mode by downward puckering of first layer Al and the 659/660 modes are more bulk in character, involving motion of first and second layer oxygen and second layer Al. Prior infrared studies of (partially) dehydrated alumina particles found a broad, weak spectral feature centered at 1000 cm^{-1} and assigned this to surface Al—O vibrations (although the high defect density of particle surfaces makes attribution to a particular molecular level motion difficult).[81] To our knowledge, no such study has appeared for any *single crystal* α-Al_2O_3 surface, presumably because of the low signal in reflection infrared measurements. As demonstrated above, VSF spectroscopy allows sampling of this mode at high signal to noise ratio for low surface area, atomically well defined alumina surfaces.

The correspondence between calculated (scaled) line spectra and experimental resonances (given in blue, Fig. 5) is less clear in case of the hydroxylated surface. At closer inspection, however, the agreement both in number and amount of

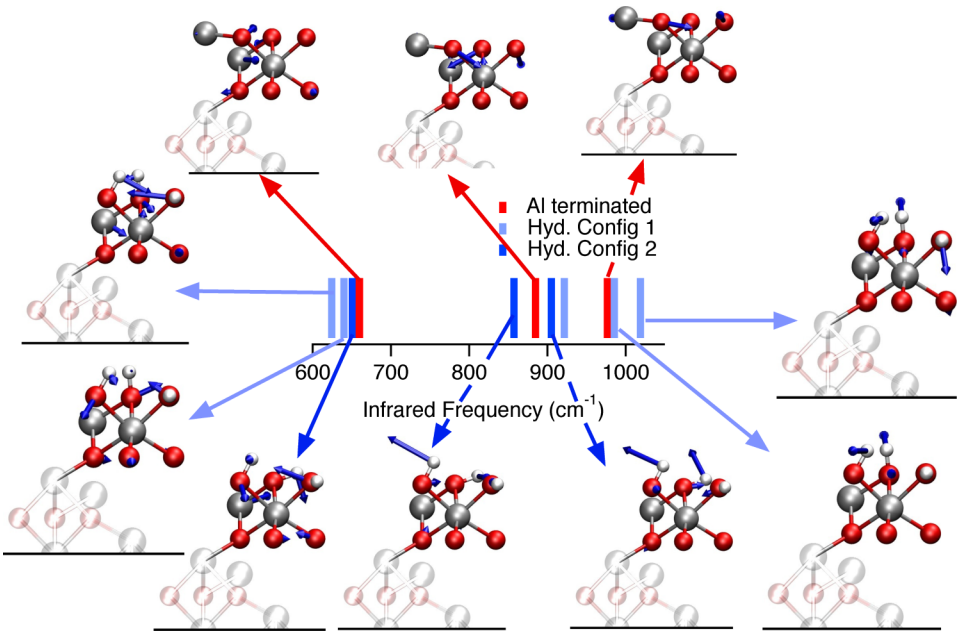

FIG. 6. Atom displacements in surface vibrational modes of 1-Al and the two possible hydroxylated surface structures.

the scaled frequencies (905, 857, and 650 cm^{-1}) in the experimental energy window seems to speak in favour of configuration 2 (featuring two in-plane hydrogen bonds), whereas the spectrum for configuration 1 (1019, 986, 921, 640, and 624 cm^{-1}) exhibits frequencies that are not observed in experiment. Given the equivalent energy of both structures, the preference for one of them is not immediately comprehensible; preliminary results based on molecular dynamics simulations presently underway in our group, however, seem to confirm this preference and tentatively suggest different vibrational anharmonicities as a possible origin.

Regarding the nature of the surface phonons, similar conclusions as for the Al-terminated surface can be drawn in case of both hydroxylated surface models. As is clear from inspection of Figure 6, the two higher energy modes for configuration 2 are dominated by the displacement of surface hydrogens, i.e., we probe the Al—O—H bend. In contrast, the mode at 650 cm^{-1} is more collective: it requires displacements of both surface hydrogens, aluminums, and second layer oxygens. For configuration 1 (in which only one OH group is in the plane of the surface), inspection of Figure 6 and the supplementary material again reveals that the three modes at higher frequencies are dominated by the displacement of the surface hydrogens, i.e., they sample the surface Al—O—H bend, whereas the lower frequency phonons are more collective in nature.[89] The assignment of the modes visible on the hydroxylated sample between 800 and 950 cm^{-1} to the surface Al—O—H bend is consistent with previous FTIR studies on boehmite (i.e., $\gamma - AlO_2H$) particles, where a weak band centered at 900 cm^{-1} was observed and found to shift to lower frequency upon surface exchange with D_2O.[82] As for the Al-terminated surface, for the hydroxylated it is clear that the lower frequency modes are complicated combinations of a larger number of atom displacements that reflect surface reconstruction more generally. Also, as for the Al-terminated sample, here the higher signal to noise of the VSF measurement makes it possible to easily probe this surface mode on the well defined, low surface area, single crystal surface allowing clear identification of the atomic motions involved.

The computational approach pursued here is clearly only a qualitative description of our measured quantities: it does not account for the symmetry restrictions of the sum frequency process (and as a result, we require a phenomenological scheme to separate surface and bulk modes) and provides no insight into mode anharmonicities, intensities, line widths, or the possible presence of combination bands. Moreover, because there is little work benchmarking the application of plane wave functionals (of any type) to compute frequencies of solid surface modes, it is difficult to quantify the model error (and to understand the offset of absolute frequencies between computation and experiment). In spite of these limitations, the qualitative insights these calculations afford are valuable: for both the Al-terminated and hydroxylated surface, the observable higher frequency modes are local, i.e., they are dominated by the Al—O vibration(s) of surface aluminum or the Al—O—H bend of surface aluminols, while the lower frequency modes of each surface involves a larger number of atoms closer to the bulk and relate to surface structure in a more collective manner.

This local nature of the higher frequency resonances suggest they should be valuable probes for surface chemistry. For the Al terminated α-Al_2O_3(0001) surface, we can now unambiguously probe the interaction of adsorbates with the reactive surface site *both* from the perspective of the adsorbate *and* the alumina. For the hydroxylated α-Al_2O_3(0001) surface, aluminol groups play an important role in almost all chemistry and thus the ability to probe them with specificity seems likely to be of general importance. In particular, for the alumina/liquid water interface surface charge development is known to occur through adsorption/desorption of H^+ on aluminols: at sufficiently low pH, Al-O-H(surf) + H^+(aq) → Al-O-H_2^+(surf), while at sufficiently high pH, Al-O-H (surf) → Al-O^-(surf) + H^+(aq).[83] Thus, we expect that extending our approach to the alumina/liquid water interface should allow direct insight into surface protonation/deprotonation, i.e., the molecular level mechanisms underlying surface charge development, not possible by other means. In addition, we note that while α-Al_2O_3(0001) has only doubly coordinated surface aluminols (i.e., surface hydroxyl groups in which the oxygen is covalently bound to two underlying aluminum atoms) other common α-Al_2O_3 surfaces, e.g., the $(1\bar{1}02)$, are more heterogeneous. We expect that the Al—O—H bend spectral response of such differently coordinated surface oxygens should differ significantly and that thus VSF measurement should provide direct insight into surface site specific pH dependent (de)protonation not possible by other means.

D. The partially hydrated α-Al_2O_3(0001) surface

To this point, we have discussed at some length, the VSF response at both Al—O and O—H frequencies characteristic of the Al terminated and hydroxylated α-Al_2O_3(0001) surface. In addition to these well-defined surface terminations, we also explored a partially hydroxylated state. As discussed above, we expect the fully hydrated sample to be covered by a combination of aluminol groups and molecularly adsorbed H_2O. Based on infrared studies of alumina powders, and work on silica,[37] we expect that minimal heating of the hydroxylated sample should lead to loss of some portion of these surface O—H populations. Provided these partially hydroxylated states have no domains larger than the laser spot size, one might expect these intermediate samples to be characterizable as a linear combination of the spectral response of the Al-terminated and hydroxylated samples.

Figure 7 shows the VSF spectral response, in the Al—O and O—H frequency ranges, for the Al-terminated and fully hydoxylated samples as well as the fully hydroxylated sample after baking for 24 h at 623 K. In both spectral ranges the heated sample is clearly intermediate between the two well-defined structural terminations. Interestingly, however, the degree to which it is intermediate differs depending on spectral window: quantitative fitting suggests that in the O—H stretch region the heated sample resonance amplitude can be well described by 90% fully hydroxylated and 10% 1-Al terminated, while in the Al—O region it can be well described by a linear combination of 40% 1-Al and 60% fully hydroxylated.

Prior work suggests the large resonance apparent in the VSF O—H stretch spectrum in air is largely the O—H stretch

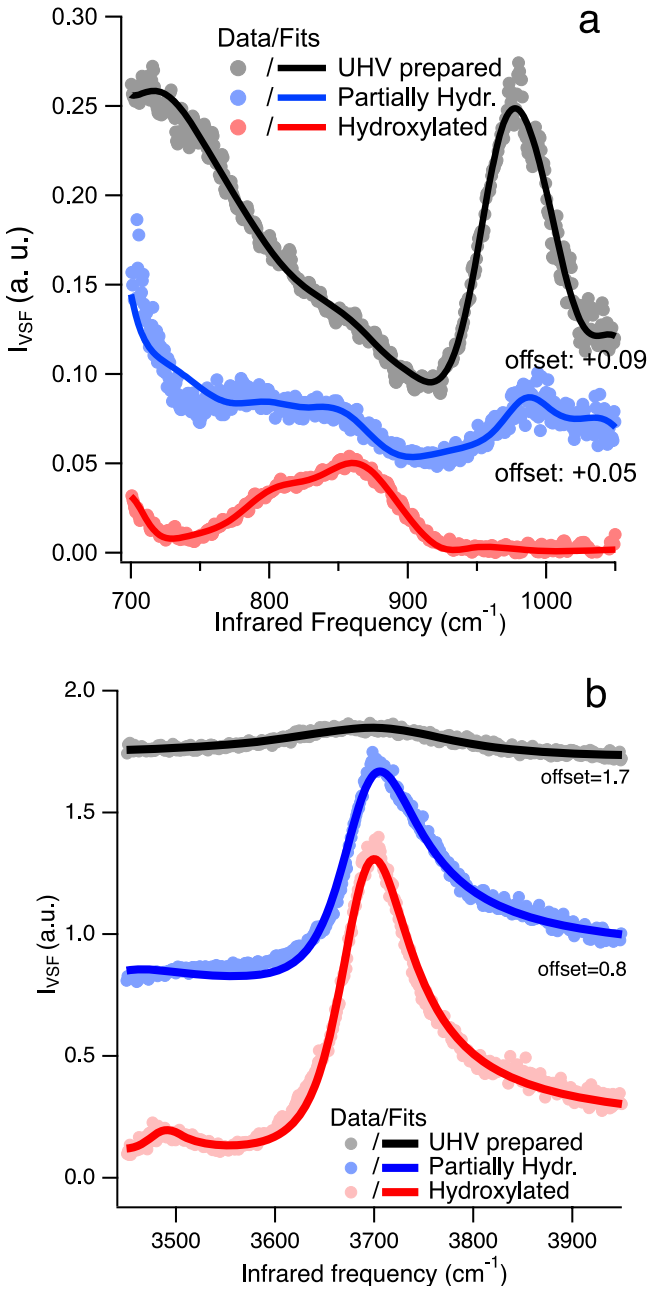

FIG. 7. (a) VSF response of the Al—O spectral region of the α-Al_2O_3(0001) surface prepared in UHV (black), fully hydroxylated (red), and fully hydroxylated sample heated at 350 °C for 24 h (blue). All spectra shown here are collected under the *ssp* polarization condition with an azimuthal angle of $\phi = 0°$.

of surface aluminols.[34] In light of this assignment, we take the decrease in this mode to be an indicator of surface dehydroxylation. In contrast, changes in the Al—O spectral response provide insight into surface structure. Evidently, the heated sample is, in some sense, structurally intermediate between our well defined terminations. Characterizing this intermediate state is challenging. Clearly, the O—H response suggests that there are large portions of the surface that remain hydroxylated. In those portions that are dehydroxylated, however, we do not expect that our α-Al_2O_3(0001) surface is 1-Al terminated. Transforming from an ideal *gibbsite-like* hydroxylated surface to the 1-Al terminated requires removing *both* surface water *and* a layer of Al_2O_3. Minimal heating in air seems unlikely to cause the later change. We are currently working on fully characterizing this structural intermediate by extending our VSF surface phonon measurements to lower frequencies to allow probing of additional surface modes. The ability to observe the full suite of surface phonons will allow us to unambiguously distinguish different possible α-Al_2O_3(0001) terminations and gain insight into how the relative abundance of different surface terminations, i.e., the size of different patches for a heterogeneous surface, change on heating.

IV. SUMMARY AND CONCLUSIONS

Water is known to dissociatively adsorb on many oxide surfaces and in doing so dramatically change a variety of surface properties. At the oxide/liquid water interface, the resulting hydroxylated surface then accepts or donates protons to bulk water as a function of pH. Both the initial adsorption of water molecules and the adsorption of protons from liquid water are coupled to structural change: adsorption leads to a rearrangement in atom positions in, at least, the first unit cell. Thus, to completely understand water/oxide interaction, we require a way of probing water and proton adsorption both from the perspective of the liquid and that of the solid. Additionally, we would like the tool we employ to do so to be suitable for analysis both in the UHV, to probe the dissociative adsorption of the initial water molecules to encounter the surface, in ambient atmospheres and at the solid/liquid water interface to probe surface (de)protonation.

Here, we accomplish these goals by characterizing the adsorption of H_2O on the α-Al_2O_3(0001) surface both from the perspective of the dissociatively adsorbed water molecule (the O—H stretch) and the solid (surface Al—O vibrations) by employing the interface specific, nonlinear optical technique, vibrational sum frequency spectroscopy. To both demonstrate the surface specificity and aid in assignment of the Al—O spectral response, we characterize the well-defined fully hydroxylated and 1-Al terminated, fully dehydroxylated, surfaces. These well-defined surface terminations make comparison with calculated normal modes possible and, therefore, enable the resulting full microscopic description of the origin of the observed resonances. Armed with this assignment we demonstrate that, viewed both from the perspective of water and the underlying solid, water dissociative adsorption on the Al terminated α-Al_2O_3(0001) surface is thermodynamically favored, but, in ambient atmospheres, quite slow. This high barrier to dissociative adsorption is presumably related to the anomalous stability of this surface in contact with liquid water at pH extremes.[84] Monitoring of the VSF O—H stretch response suggests that, on mild heating, we create an α-Al_2O_3(0001) surface that is partially dehydroxylated. Concurrent monitoring of the VSF Al—O spectral response gives insight into the manner in which the dehydroxylated portion of the surface reconstructs (the sample evolves towards the spectral response of the UHV prepared surface). We are currently working on extending the surface phonon measurements described here to lower frequencies to both fully characterize the surface termination of the dehydroxylated portion of the surface and to

quantify the relative ratios of the various surface terminations, e.g., 1-Al, 2-Al, hydroxylated, etc., as a function of heating.

For decades, macroscopic properties of oxide/water interfaces—acid/base titrations, electrokinetic properties, ion adsorption—have been measured. For more than thirty years, it has been recognized that such macroscopic measurements reflect a sum of surface sites that may have quite different properties (i.e., acidities, polarities, etc.) and that inferring properties of surface site types from these macroscopic measurements is not possible.[85,86] While a variety of theoretical and computational approaches have proven useful in gaining additional insight,[5,87,88] finding site specific experimental constraints, e.g., probing the protonation of particular types of surface sites with changing pH, has proven challenging. Much of the problem here is technical, most methods are either insensitive to hydrogen, not capable of unambiguously distinguishing the O—H groups of molecularly from those of dissociatively adsorbed water or both. Extension of the measurements described in this study to the α-alumina/liquid water interface, as well as other oxide systems, seems poised to overcome these challenges and thus significantly alter our knowledge of the oxide/water interface.

ACKNOWLEDGMENTS

Y.T. thanks Claude Monney for his careful proofreading of the manuscript. All authors thank the Deutsche Forschungsgemeinschaft for their support of this project through Collaborative Research Center 1109: Understanding of Metal Oxide/Water Systems at the Molecular Scale: Structural Evolution, Interfaces and Dissolution.

[1]V. E. Henrich and P. A. Cox, *The Surface Science of Metal Oxides* (Cambridge University Press, 1996).
[2]G. E. Brown, V. E. Henrich, W. H. Casey, D. L. Clark, C. Eggleston, A. Felmy, D. W. Goodman, M. Grätzel, G. Maciel, and M. I. McCarthy, Chem. Rev. **99**, 77 (1999).
[3]H. A. Al-Abadleh and V. H. Grassian, Surf. Sci. Rep. **52**, 63 (2003).
[4]U. Diebold, S.-C. Li, and M. Schmid, Annu. Rev. Phys. Chem. **61**, 129 (2010).
[5]T. Hiemstra, W. H. van Riemsdijk, and G. H. Bolt, J. Colloid Interface Sci. **133**, 91 (1989).
[6]T. Hiemstra and W. H. Van Riemsdijk, J. Colloid Interface Sci. **179**, 488 (1996).
[7]D. A. Sverjensky, Geochim. Cosmochim. Acta **69**, 225 (2005).
[8]J. W. Elam, C. E. Nelson, M. A. Cameron, M. A. Tolbert, and S. M. George, J. Phys. Chem. B **102**, 7008 (1998).
[9]P. Guenard, G. Renaud, A. Barbier, and M. Gautier-Soyer, Surf. Rev. Lett. **5**, 321 (1998).
[10]G. Renaud, Surf. Sci. Rep. **32**, 5 (1998).
[11]M. Ricci, P. Spijker, F. Stellacci, J.-F. Molinari, and K. Voïtchovsky, Langmuir **29**, 2207 (2013).
[12]I. Siretanu, D. Ebeling, M. P. Andersson, S. L. S. Stipp, A. Philipse, M. C. Stuart, D. van den Ende, and F. Mugele, Sci. Rep. **4**, 4954 (2014).
[13]H. A. Al-Abadleh and V. H. Grassian, Langmuir **19**, 341 (2003).
[14]A. C. Thomas and H. H. Richardson, J. Phys. Chem. C **112**, 20033 (2008).
[15]Y. R. Shen, Nature **337**, 519 (1989).
[16]C. D. Bain, J. Chem. Soc., Faraday Trans. **91**, 1281 (1995).
[17]K. B. Eisenthal, Chem. Rev. **96**, 1343 (1996).
[18]M. J. Shultz, C. Schnitzer, D. Simonelli, and S. Baldelli, Int. Rev. Phys. Chem. **19**, 123 (2000).
[19]Z. Chen, Y. R. Shen, and G. A. Somorjai, Annu. Rev. Phys. Chem. **53**, 437 (2002).
[20]G. L. Richmond, Chem. Rev. **102**, 2693 (2002).
[21]H.-F. Wang, W. Gan, R. Lu, Y. Rao, and B.-H. Wu, Int. Rev. Phys. Chem. **24**, 191 (2005).
[22]S. Gopalakrishnan, D. F. Liu, H. C. Allen, M. Kuo, and M. J. Shultz, Chem. Rev. **106**, 1155 (2006).
[23]Y. R. Shen and V. Ostroverkhov, Chem. Rev. **106**, 1140 (2006).
[24]S. Ye and M. Osawa, Chem. Lett. **38**, 386 (2009).
[25]S. Roke, ChemPhysChem **10**, 1380 (2009).
[26]F. M. Geiger, Annu. Rev. Phys. Chem. **60**, 61 (2009).
[27]J. F. D. Liljeblad and E. Tyrode, J. Phys. Chem. C **116**, 22893 (2012).
[28]E. Tyrode and J. F. Liljeblad, J. Phys. Chem. C **117**, 1780 (2013).
[29]S. Kataoka, M. Gurau, F. Albertorio, M. Holden, S. Lim, R. Yang, and P. Cremer, Langmuir **20**, 1662 (2004).
[30]I. Li, J. Bandura, and M. J. Shultz, Langmuir **20**, 10474 (2004).
[31]V. Ostroverkhov, G. A. Waychunas, and Y. Shen, Chem. Phys. Lett. **386**, 144 (2004).
[32]C. Wang, H. Groenzin, and M. Shultz, J. Phys. Chem. B **108**, 265 (2004).
[33]V. Ostroverkhov, G. A. Waychunas, and Y. Shen, Phys. Rev. Lett. **94**, 046102 (2005).
[34]L. Zhang, C. Tian, G. A. Waychunas, and Y. R. Shen, J. Am. Chem. Soc. **130**, 7686 (2008).
[35]M. Flörsheimer, K. Kruse, R. Polly, A. Abdelmonem, B. Schimmelpfennig, R. Klenze, and T. Fanghänel, Langmuir **24**, 13434 (2008).
[36]B. Braunschweig, S. Eissner, and W. Daum, J. Phys. Chem. C **112**, 1751 (2008).
[37]W. T. Liu and Y. R. Shen, Phys. Rev. Lett. **101**, 016101 (2008).
[38]J. A. Kelber, Surf. Sci. Rep. **62**, 271 (2007).
[39]C. Morterra and G. Magnacca, Catal. Today **27**, 497 (1996).
[40]W. T. Liu and Y. R. Shen, Phys. Rev. B **78**, 024302 (2008).
[41]Y. Tong, Y. Zhao, N. Li, M. Osawa, P. B. Davies, and S. Ye, J. Chem. Phys. **133**, 034704 (2010).
[42]Y. Tong, A. Vila Verde, and R. K. Campen, J. Phys. Chem. B **117**, 11753 (2013).
[43]H. Held, A. Lvovsky, X. Wei, and Y. Shen, Phys. Rev. B **66**, 205110 (2002).
[44]C. D. Bain, P. B. Davies, T. H. Ong, R. N. Ward, and M. A. Brown, Langmuir **7**, 1563 (1991).
[45]A. S. Barker, Jr., Phys. Rev. **132**, 1474 (1963).
[46]E. D. Palik, *Handbook of Optical Constants of Solids: Index* (Elsevier, 1998), Vol. 3.
[47]M. Schubert, T. E. Tiwald, and C. M. Herzinger, Phys. Rev. B **61**, 8187 (2000).
[48]W. Kohn and L. J. Sham, Phys. Rev. **140**, A1133 (1965).
[49]P. E. Blöchl, Phys. Rev. B **50**, 17953 (1994).
[50]G. Kresse and D. Joubert, Phys. Rev. B **59**, 1758 (1999).
[51]G. Kresse and J. Hafner, Phys. Rev. B **47**, 558 (1993).
[52]G. Kresse and J. Hafner, Phys. Rev. B **48**, 13115 (1993).
[53]G. Kresse and J. Hafner, Phys. Rev. B **49**, 14251 (1994).
[54]J. P. Perdew, K. Burke, and M. Ernzerhof, Phys. Rev. Lett. **77**, 3865 (1996).
[55]J. P. Perdew, K. Burke, and M. Ernzerhof, Phys. Rev. Lett. **78**, 1396 (1997).
[56]S. Grimme, J. Comput. Chem. **27**, 1787 (2006).
[57]H. J. Monkhorst and J. D. Pack, Phys. Rev. B **13**, 5188 (1976).
[58]P. Thompson, D. E. Cox, and J. B. Hastings, J. Appl. Crystallogr. **20**, 79 (1987).
[59]K. C. Hass, W. F. Schneider, A. Curioni, and W. Andreoni, Science **282**, 265 (1998).
[60]V. A. Ranea, I. Carmichael, and W. F. Schneider, J. Phys. Chem. C **113**, 2149 (2009).
[61]Z. Łodziana, J. K. Nørskov, and P. Stoltze, J. Chem. Phys. **118**, 11179 (2003).
[62]C. Klein and C. S. Hurlburt, Jr., *Manual of Mineralogy* (John Wiley and Sons Inc., New York, Chichester, Brisbane, Toronto, Singapore, 1993), Vol. 21.
[63]S. P. S. Porto and R. S. Krishnan, J. Chem. Phys. **47**, 1009 (1967).
[64]M. C. Munisso, W. Zhu, and G. Pezzotti, Phys. Status Solidi B **246**, 1893 (2009).
[65]C. Hirose, N. Akamatsu, and K. Domen, Appl. Spectrosc. **46**, 1051 (1992).
[66]S. Malyk, F. Y. Shalhout, L. E. O'Leary, N. S. Lewis, and A. V. Benderskii, J. Phys. Chem. C **117**, 935 (2013).
[67]T. Kurita, K. Uchida, and A. Oshiyama, Phys. Rev. B **82**, 155319 (2010).
[68]E. A. Soares, M. A. Van Hove, C. F. Walters, and K. F. McCarty, Phys. Rev. B **65**, 195405 (2002).
[69]P. Liu, T. Kendelewicz, G. E. Brown, E. J. Nelson, and S. A. Chambers, Surf. Sci. **417**, 53 (1998).
[70]C. Niu, K. Shepherd, D. Martini, J. Tong, J. A. Kelber, D. R. Jennison, and A. Bogicevic, Surf. Sci. **465**, 163 (2000).
[71]J. A. Kelber, C. Niu, K. Shepherd, D. R. Jennison, and A. Bogicevic, Surf. Sci. **446**, 76 (2000).

[72]Q. Fu, T. Wagner, and M. Rühle, Surf. Sci. **600**, 4870 (2006).
[73]H. Kirsch, J. Wirth, Y. Tong, M. Wolf, P. Saalfrank, and R. K. Campen, J. Phys. Chem. C **118**, 13623 (2014).
[74]P. J. Eng, T. P. Trainor, G. E. Brown, Jr., G. A. Waychunas, M. Newville, S. R. Sutton, and M. L. Rivers, Science **288**, 1029 (2000).
[75]M. Liehr, P. A. Thiry, J. J. Pireaux, and R. Caudano, J. Vac. Sci. Technol. A **2**, 1079 (1984).
[76]R. Fuchs and K. L. Kliewer, Phys. Rev. **140**, A2076 (1965).
[77]A. A. Lucas and M. Šunjić, Prog. Surf. Sci. **2**, 75 (1972).
[78]M. Frank, K. Wolter, N. Magg, M. Heemeier, R. Kühnemuth, M. Bäumer, and H.-J. Freund, Surf. Sci. **492**, 270 (2001).
[79]X. G. Wang, A. Chaka, and M. Scheffler, Phys. Rev. Lett. **84**, 3650 (2000).
[80]A. Marmier and S. C. Parker, Phys. Rev. B **69**, 115409 (2004).
[81]J.-C. Lavalley and M. Benaissa, J. Chem. Soc., Chem. Commun. **1984**, 908.
[82]C. Morterra, C. Emanuel, G. Cerrato, and G. Magnacca, J. Chem. Soc., Faraday Trans. **88**, 339 (1992).
[83]C. Contescu, J. Jagiello, and J. A. Schwarz, Langmuir **9**, 1754 (1993).
[84]J. Lützenkirchen, R. Zimmermann, T. Preočanin, A. Filby, T. Kupcik, D. Küttner, A. Abdelmonem, D. Schild, T. Rabung, and M. Plaschke, Adv. Colloid Interface Sci. **157**, 61 (2010).
[85]J. Westall and H. Hohl, Adv. Colloid Interface Sci. **12**, 265 (1980).
[86]G. Sposito, Adv. Colloid Interface Sci. **91**, 329 (1983).
[87]T. Hiemstra, J. C. M. de Wit, and W. H. van Riemsdijk, Adv. Colloid Interface Sci. **133**, 105 (1989).
[88]M. L. Machesky, M. Predota, D. J. Wesolowski, L. Vlcek, P. T. Cummings, J. Rosenqvist, M. K. Ridley, J. D. Kubicki, A. V. Bandura, N. Kumar, and J. O. Sofo, Langmuir **24**, 12331 (2008).
[89]See supplementary material at http://dx.doi.org/10.1063/1.4906346 for details of line shape model and data analysis, azimuthal dependent VSF spectra of the hydroxylated sample under the *ssp* polarization condition in the Al—O frequency region and parameters resulting from fits to this data, parameters resulting from the analysis of VSF spectra collected from the 1-Al terminated sample in the Al—O frequency region under the *ssp* polarization condition, VSF spectra and parameters resulting from fits of VSF spectra collected from both the hydroxylated and 1-Al terminated samples under the *pps*, *psp*, *spp* and *ppp* polarization conditions in the Al—O frequency region, parameters resulting from analysis of the VSF spectra collected from the 1-Al terminated and hydroxylated samples in the OH stretch region, a simulated EELS spectrum for the α-Al_2O_3(0001) surface, additional illustrations of atom displacements associated with calculated normal modes and details of the selection criteria employed to determine surface phonons.